Research Article

Chi Li, Zai-Quan Xu*, Noah Mendelson, Mehran Kianinia, Milos Toth and Igor Aharonovich*

Purification of single-photon emission from hBN using post-processing treatments

https://doi.org/10.1515/nanoph-2019-0099
Received April 1, 2019; revised June 26, 2019; accepted July 2, 2019

Abstract: Single-photon emitters (SPEs) in hexagonal boron nitride (hBN) are promising components for on-chip quantum information processing. Recently, large-area hBN films prepared by chemical vapor deposition (CVD) were found to host uniform, high densities of SPEs. However, the purity of these emitters has, to date, been low, hindering their applications in practical devices. In this work, we present two methods for post-growth processing of hBN, which significantly improve SPEs in hBN films that had been transferred from substrates used for CVD. The emitters exhibit high photon purities in excess of 90% and narrow linewidths of ~3 nm at room temperature. Our work lays a foundation for producing high-quality emitters in an ultra-compact two-dimensional material system and paves the way for deployment of hBN SPEs in scalable on-chip photonic and quantum devices.

Keywords: hexagonal boron nitride; single-photon emitters; two-dimensional materials; thermal annealing; UV ozone.

1 Introduction

Solid-state single-photon emitters (SPEs) are sought after for a plethora of applications in quantum technologies [1–3]. Hexagonal boron nitride (hBN) has recently emerged as a source of bright and photostable SPEs that operate at room temperature [4–13]. Since then, tremendous efforts have been devoted to the fabrication and optimization of SPEs in hBN crystals of various sizes and geometries. Efforts to engineer SPEs in hBN have employed molecular beam epitaxy and chemical vapor deposition (CVD) growth techniques, as well as a range of electron irradiation, laser processing, ion implantation, wet etching, annealing and plasma processing methods [14–19].

Of the above-mentioned techniques, the CVD process is attractive, as it enables growth of large-area hBN films that can host a high density of SPEs [15]. However, employment of these hBN films in practical devices often requires transfer of the hBN from the substrate used for CVD and subsequent lithographic patterning processes. This typically generates residual organic contaminants that degrade SPEs. Methods to remove such contaminants from materials like graphene and other two-dimensional (2D) transition metal dichalcogenides were previously investigated [20, 21]. For instance, thermal annealing was effective to remove organic contaminants from hBN [22]. Very recently, a poly(vinyl acetate) (PVA) stamp peeling transfer of hBN grown on Pt foil was proposed to minimize interfacial contamination during the transfer process [23]. However, little is known about their effects on the performance of SPEs in hBN.

In this work, we present two practical, reliable methods to achieve high purity of SPEs in hBN – namely, high-temperature annealing in air and ultraviolet (UV) ozone processing. Both methods are highly effective at improving the optical quality, namely, photon purity and linewidth of the zero phonon line (ZPL), of CVD-grown hBN and yield SPEs with room-temperature linewidths of ~3 nm and autocorrelation curves with zero-delay-time intensities of ≤0.1. A large enhancement in SPE quality is ascribed to the removal of organic residues from the hBN surface. The presented treatments are compatible with the techniques for integration of hBN with other 2D materials and photonic resonators.

***Corresponding authors: Zai-Quan Xu and Igor Aharonovich,** School of Mathematical and Physical Sciences, University of Technology Sydney, 15 Broadway, Ultimo, 2007 NSW, Australia, e-mail: zaiquan.xu@uts.edu.au (Z.-Q. Xu); igor.aharonovich@uts.edu.au (I. Aharonovich)
Chi Li, Noah Mendelson, Mehran Kianinia and Milos Toth: School of Mathematical and Physical Sciences, University of Technology Sydney, 15 Broadway, Ultimo, 2007 NSW, Australia

2 Materials and methods

2.1 hBN transfer

Multilayer hBN films grown by CVD on 50-μm copper foils were purchased from Graphene Supermarket (product number CVD-2X1-BN-ML). The films were transferred using a poly(methyl methacrylate) (PMMA)-assisted wet transfer method [24] (transfer details are provided in Figure S1). First, PMMA (A4, Microchem) was spin coated on hBN and heated to 130°C for 20 min to evaporate the solvent. Cu foil was then etched by floating the hBN/PMMA film in a warm (80°C) 0.5 M aqueous ammonium persulfate solution for 1 h. The remaining hBN/PMMA film was subsequently rinsed three times with deionized (DI) water before loading onto a clean Si substrate with a 300-nm thermal oxide layer (Si/SiO_2). The samples were dried in a small vacuum desiccator before subsequently heated to 120°C for 30 min to ensure adherence between the hBN and SiO_2 surface. The PMMA layer was then removed by immersing the samples in warm acetone and *N*-methyl-2-pyrrolidone solvent for 30 min each. Finally, the hBN films were rinsed with isopropanol and DI water before being blow-dried with nitrogen.

2.2 Annealing and UV ozone treatment

2.2.1 High-temperature annealing

Transferred samples were put into a tube furnace and annealed for 3 h in air at 350, 550 or 750°C (denoted as hBN-350, hBN-550 and hBN-750, respectively). The samples were then cooled to room temperature at ~10°C/min.

2.2.2 UV ozone treatment

Transferred samples were heated to 120°C on a hotplate for an hour before being placed in an UV ozone cleaner (ProCleaner™ Plus, Bioforce Nanosciences Inc.) and ozone processed for 15, 30 or 60 min.

The morphology of hBN films was characterized using the tapping mode of an atomic force microscope (Veeco Dimension 3100).

3 Results and discussions

We systematically investigated two approaches (thermal annealing in air and UV ozone treatment) for removing the residual polymer present after transfer of hBN from CVD growth substrates and the subsequent effects on the optical performance of SPEs. Figure 1A is a schematic illustration of the annealing method. The CVD hBN films on Si/SiO_2 were annealed in air at 350, 550, or 750°C. After annealing, SPE properties were investigated at room temperature using a custom-built confocal setup. We were not able to find SPEs in hBN-350 (Figure S2) and untreated hBN film (Figure S3) even though we could record photoluminescence (PL) emissions that resemble those of SPEs. However, samples annealed at 550 and 750°C do contain SPEs. Figure 1B shows typical spectra of SPEs after annealing at 550 (black) and 750°C (red). The full width at half maximum (FWHM) of the ZPLs in Figure 1B, extracted from a single Lorentzian fit, yielded values of 18 and 4 nm for hBN-550 and hBN-750, respectively. Additional peaks red shifted by $\gtrsim$160 meV from the ZPL are phonon sidebands [25, 26].

Importantly, the background fluorescence contribution to the recorded emissions is significantly reduced in the sample annealed at 750°C. This was further confirmed by measuring second-order autocorrelation functions [$g^2(\tau)$] using a Hanbury-Brown-Twiss interferometer. Figure 2C shows a $g^2(0)$ curve obtained by a pulsed excitation laser with a best $g^2(0)$ value of 0.07 ± 0.03. Such a low $g^2(0)$ value is highly advantageous for practical applications in communications and quantum key distribution [27].

Pulsed photon autocorrelation data (Figure 1C) were fitted with single exponential function. An n-peak fitting function is defined below

$$D(t) = \sum_{0}^{n} (a + b_n * \exp(-|(t - t_n) / \mathrm{tau}_n|))$$

in which n is the peak number, parameter a is a constant baseline, b_n is the peak height factor, t_n stands for peak center position and tau_n is the corresponding decay lifetime. By calculating the standard deviation of the peak height and the baseline, we determined that the slightly random height difference resulted from the system response (bin width for the shown data is 64 ps). To get better overlap and more precise peak area, we fixed the height factor (b_n) for each peak to their maximum values. Once acquiring a, b_n, t_n and tau_n, the nth peak area was calculated by integral in the $[t_n - 30, t_n + 30]$ region, namely

$$A_n = \int_{t_n - 30}^{t_n + 30} (a + b_n * \exp(-|(t - t_n) / \mathrm{tau}_n|)) dt$$

The value of $g^2(0)$ is defined as the ratio $\frac{A_0}{A_{\mathrm{adj.}}}$, where A_0 and $A_{\mathrm{adj.}}$ are the area under the curve of the peak at

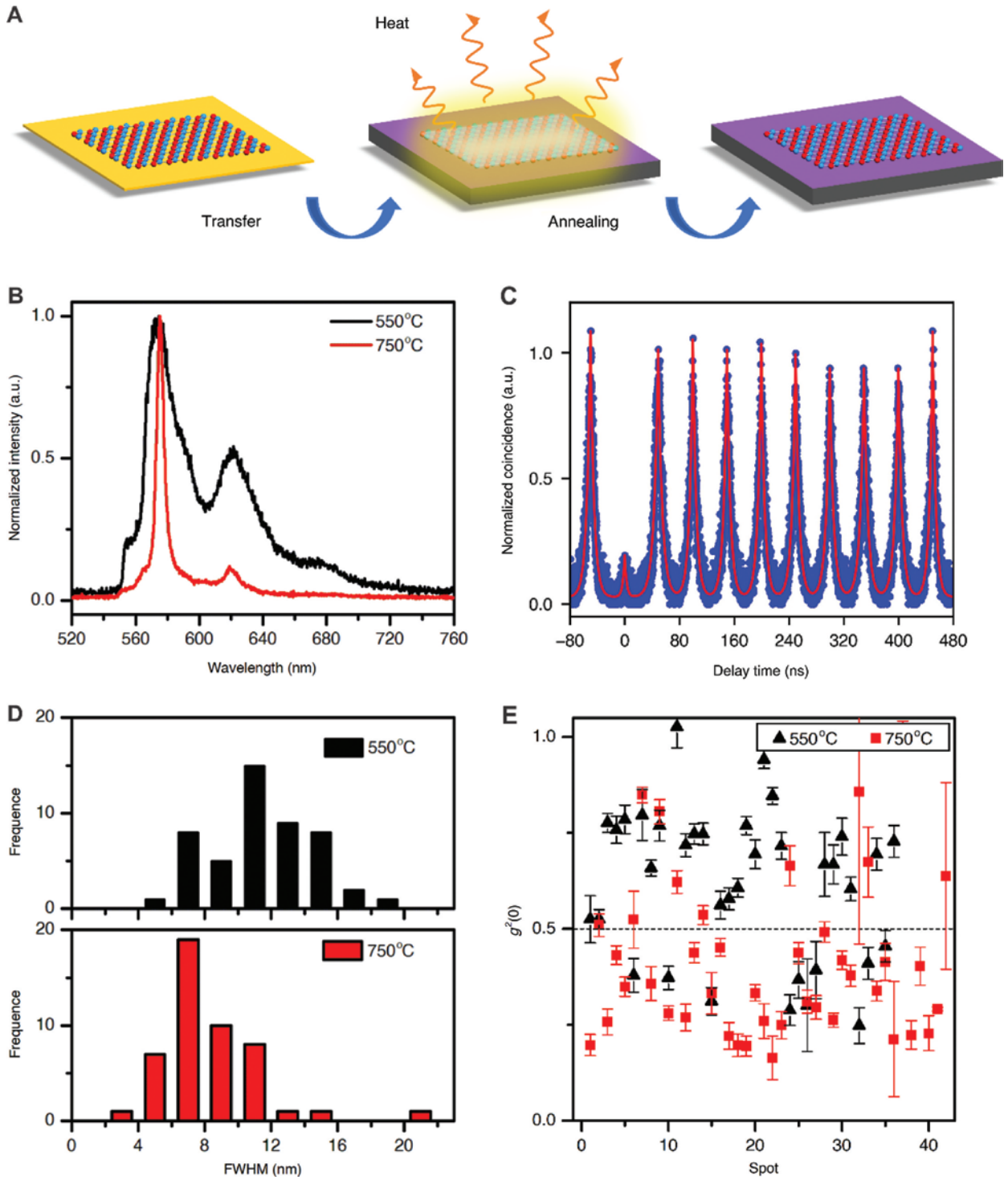

Figure 1: Room-temperature optical characterizations of annealed CVD hBN films.
(A) Schematic illustration of the thermal annealing process. hBN films were transferred from copper substrates to Si/SiO_2 (300 nm) substrates and subsequently annealed at high temperatures prior to optical measurements. (B) Normalized PL spectra of a representative SPE from hBN annealed at 550°C (black) and 750°C (red). The ZPLs have an FWHM of ~18.0 and 4.0 nm, respectively. (C) Autocorrelation curve obtained from an emitter that was annealed at 750°C. The excitation source was a 20-MHz, 512-nm pulsed laser. The intensity at zero delay time [$g^2(0)$] is 0.07 ± 0.03 (without background correction) at room temperature. Red curve is fitted data by single exponential decay function. (D) Histograms of the FWHM of SPE emission lines from hBN samples annealed at 550°C (red) and 750°C (black). The average FWHM are 11.9 and 8.1 nm, respectively. (E) Scatter plot of $g^2(0)$ values from emitters from corresponding samples shown in (D). Average $g^2(0)$ values are 0.62 ± 0.19 and 0.41 ± 0.20 for hBN-550 and hBN-750, respectively.

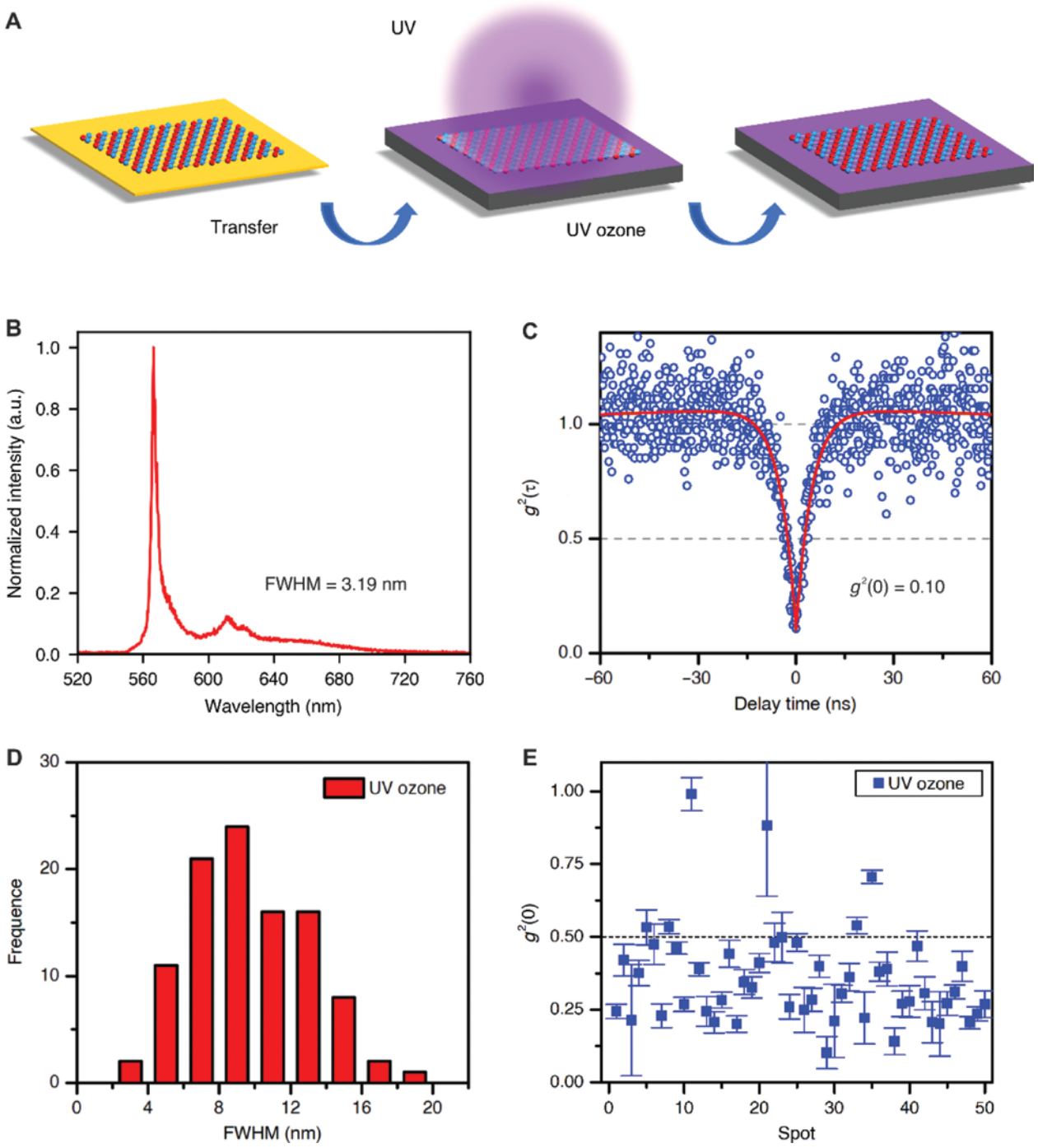

Figure 2: Room-temperature optical characterizations of hBN films that were processed by UV ozone.
(A) Schematic illustration of the UV ozone treatment. (B) Normalized PL spectrum of a representative SPE. The ZPL is centered at 567.1 nm with an FWHM of 3.19 nm. (C) Autocorrelation measurement of the emitter excited by a 532-nm CW laser. The intensity at zero delay time [$g^2(0)$] is 0.10 ± 0.04 (without background correction). (D) Histogram of the FWHM of 100 emitters. The average FWHM is ~9.0 nm. (E) Scatter plot of $g^2(0)$ values from the same group of samples shown in (D), showing that 88% of the emissions are from SPEs. Average $g^2(0)$ value is 0.36 ± 0.17. Error bars plotted are derived from corresponding fitting uncertainties.

zero delay time and the peak adjacent to it, respectively. For precision concern, the $A_{adj.}$ here is extracted from the average area value of 10 adjacent pulse peak areas.

To demonstrate the quality of the SPEs obtained by the 550 and 750°C annealing treatments statistically, we compared the FWHM and the $g^2(0)$ values of 107

emitters in Figure 1D and E, respectively. Note that these autocorrelation curves were obtained by a continuous-wave excitation laser, and the data were not background corrected. Corresponding experimental data (same to Figures 2C and E and S4) were fitted by a three-level model,

$$g^2(t) = a - (1+b)\exp\left(\frac{-|t|}{\text{tau}_1}\right) + b * \exp\left(\frac{-|t|}{\text{tau}_2}\right)$$

where tau_1 and tau_2 are related to decay rates of the excited and metastable states, respectively. Parameters a and b are fitting parameters. All of the parameters were set to free during the fitting process. After fitting the experimental data, the $g^2(0)$ was extracted at time $t = 0$. Figure 1D shows a histogram of the FWHM of the emitters in hBN-550 (black) and hBN-750 (red). The average FWHM from hBN-750 is 8.1 nm, while the value is 11.9 nm for hBN-550, showing that the higher annealing temperature clearly yields narrower spectral line widths. Similarly, in hBN-550, the average $g^2(0)$ value, 0.62 ± 0.19, is greater than 0.5, suggesting that most of the emissions are compromised by significant background fluorescence, while in hBN-750, the fraction of emissions with a $g^2(0)$ value, 0.41 ± 0.20, of less than 0.5 is significantly increased. Overall, 74% of the emitters in hBN-750 are SPEs [defined by $g^2(0) < 0.5$], while only 32.1% are SPEs in hBN-550. Thermal annealing is therefore a robust, scalable method for producing high-quality SPEs in post-transferred CVD-grown hBN.

Next, we present an alternative approach for improving SPE quality that does not require high temperatures but is instead based on oxidation in ozone. The procedure is shown schematically in Figure 2A. As-transferred hBN was placed into an UV ozone cleaner to remove polymer residues from the hBN surface. UV ozone cleaning employs highly reactive oxygen radicals to oxidize sp^3-hybridized carbon, thereby breaking up PMMA chains and converting them into volatile species [28]. UV-ozone-cleaned hBN displays an abundance of high-quality SPEs despite the absence of high-temperature processing. A representative spectrum, showing a sharp ZPL at 566.8 nm and an FWHM of ~3.19 nm, is shown in Figure 2B. As in the annealed samples, a phonon sideband is red shifted by ~160 meV from the ZPL. An autocorrelation curve from this emitter is shown in Figure 2C and has a best $g^2(0)$ value of 0.10 ± 0.04. This suggests that the effectiveness of the low-temperature ozone treatment is similar to that of high-temperature annealing in terms of generation of high-quality SPEs in hBN.

We studied 100 emitters in this sample to illustrate the statistical validity of the ozone process. A histogram of the FWHM of the emitters is shown in Figure 2D. It has an average FWHM of 9 nm, which is comparable to hBN-550 (Figure 1D, bottom). Interestingly, the autocorrelation measurements from the UV ozone hBN reveal that 88% of the emitters have $g^2(0)$ values, average of 0.36 ± 0.17, below 0.5, indicating efficient suppression of background fluorescence (Figure 2E). UV ozone cleaning is therefore an effective method for producing high-quality SPEs in CVD hBN, providing a low temperature alternative to annealing at/above 550°C. Data from hBN processed by the UV ozone for 15, 30 and 60 min are in Figure S4.

In order to provide insights into the morphological changes produced by the annealing and ozone treatments, we conducted atomic force microscopy (AFM) measurements at the flake edges of hBN. Figure 3A and B shows AFM traces performed on hBN after thermal

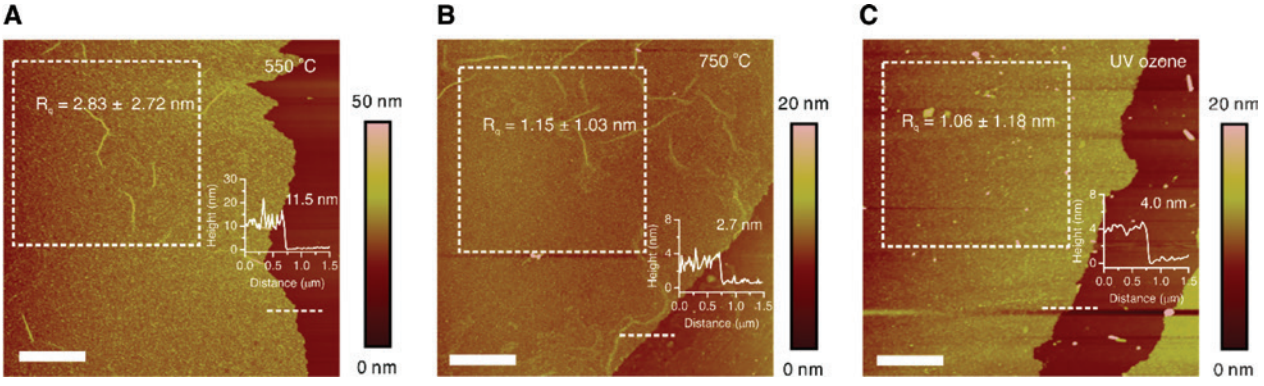

Figure 3: AFM traces of hBN after post-transfer processing.
The results in (A) and (B) were collected from samples after annealing at 550 and 750°C, respectively. Scale bar: 2 μm. The results in (C) were obtained from a sample after UV ozone cleaning. Scale bar: 2 μm. Dashed lines on the sample edge indicate where the height profiles were collected, while the dashed box defines the area where the roughness values were collected.

annealing at 550 and 750°C, respectively. Similar data from a UV-ozone-treated sample are shown in Figure 3C. The white boxes and dashed horizontal lines indicate the areas where surface roughness and height profiles were measured, respectively. The height profiles are shown as insets. Occasional wrinkles (seen in Figure 3A and B) are attributed to water trapped at the film/substrate interface based on previous reports [29, 30]. Both the roughness and flake thicknesses decrease with increasing annealing temperature – the roughness (R_q) decreases from 4.21 nm (Figure S2C) to 1.15 nm. The samples that were annealed at 750°C and ozone processed (Figure 3B and C) both have similar, low surface roughness of ~1 nm and also contain the best-quality SPEs. Accordingly, a smoother surface together with a higher signal-to-noise ratio was revealed by the confocal scan in Figure S5C and D. We also noticed that there are other methods for transferring hBN using PVA, which can reduce the polymer residuals; however, a post-transfer treatment allows further purification of the SPEs (Figure S6).

4 Conclusions

In conclusion, we systematically investigated two different methods for removing residual polymers on as-transferred hBN and the effects that this has on the optical properties of SPEs. The first approach is based on high-temperature annealing in air. The purity of SPEs can be as low as 0.07 ± 0.03 based on autocorrelation measurements. However, processing at high temperatures is not compatible with some on-chip device fabrication methods, and a second approach was therefore demonstrated to provide a low-temperature alternative. In this approach, residuals are removed by the UV ozone. We also observed a reduction in the FWHM of emitters after processing, which is likely caused, in part, by modification of the local environment of the emitters. Our work provides a versatile template for the preparation and cleaning of CVD-grown hBN after transferring, which is a vital step for the fabrication of devices based on SPEs in hBN.

Acknowledgments: We thank T. T. Tran for assistance in the data analysis and the fruitful discussions. We also thank H. Duong, M. Nguyen, J. Froch and S. Kim for their help with the optical measurements, and C. Bradac for useful discussions. The financial support from the Australian Research Council (via DP190101058, DP180100077 and LP170100150) is gratefully acknowledged.

References

[1] Atatüre M, Englund D, Vamivakas N, et al. Material platforms for spin-based photonic quantum technologies. Nat Rev Mater 2018;3:38.
[2] Senellart P, Solomon G, White A. High-performance semiconductor quantum-dot single-photon sources. Nat Nanotechnol 2017;12:1026.
[3] Toth M, Aharonovich I. Single photon sources in atomically thin materials. Annu Rev Phys Chem 2019;70:123–42.
[4] Tran TT, Bray K, Ford MJ, et al. Quantum emission from hexagonal boron nitride monolayers. Nat Nanotechnol 2016;11:37–41.
[5] Proscia NV, Shotan Z, Jayakumar H, et al. Near-deterministic activation of room temperature quantum emitters in hexagonal boron nitride. Optica 2018;5:1128.
[6] Jungwirth NR, Calderon B, Ji Y, et al. Temperature dependence of wavelength selectable zero-phonon emission from single defects in hexagonal boron nitride. Nano Lett 2016;16:6052–7.
[7] Schell AW, Svedendahl M, Quidant R. Quantum emitters in hexagonal boron nitride have spectrally tunable quantum efficiency. Adv Mater 2018;30:1704237.
[8] Exarhos AL, Hopper DA, Patel RN, et al. Magnetic-field-dependent quantum emission in hexagonal boron nitride at room temperature. Nat Commun 2019;10:222.
[9] Kianinia M, Regan B, Tawfik SA, et al. Robust solid-state quantum system operating at 800 K. ACS Photonics 2017;4:768–73.
[10] Feng J, Deschout H, Caneva S, et al. Imaging of optically active defects with nanometer resolution. Nano Lett 2018;18:1739.
[11] Koperski M, Nogajewski K, Potemski M. Single photon emitters in boron nitride: more than a supplementary material. Opt Commun 2018;411:158–65.
[12] Li X, Shepard GD, Cupo A, et al. Nonmagnetic quantum emitters in boron nitride with ultranarrow and sideband-free emission spectra. ACS Nano 2017;11:6652–60.
[13] Martínez LJ, Pelini T, Waselowski V, et al. Efficient single photon emission from a high-purity hexagonal boron nitride crystal. Phys Rev B 2016;94:121405.
[14] Vogl T, Campbell G, Buchler BC, et al. Fabrication and deterministic transfer of high-quality quantum emitters in hexagonal boron nitride. ACS Photonics 2018;5:2305–12.
[15] Mendelson N, Xu ZQ, Tran TT, et al. Engineering and tuning of quantum emitters in few-layer hexagonal boron nitride. ACS Nano 2019;13:3132–40.
[16] Ngoc My Duong H, Nguyen MAP, Kianinia M, et al. Effects of high-energy electron irradiation on quantum emitters in hexagonal boron nitride. ACS Appl Mater Interfaces 2018;10:24886–91.
[17] Xu Z-Q, Elbadawi C, Tran TT, et al. Single photon emission from plasma treated 2D hexagonal boron nitride. Nanoscale 2018;10:7957–65.
[18] Hernández-Mínguez A, Lähnemann J, Nakhaie S, et al. Luminescent defects in a few-layer h-BN film grown by molecular beam epitaxy. Phys Rev Appl 2018;10:044031.
[19] Grosso G, Moon H, Lienhard B, et al. Tunable and high-purity room temperature single-photon emission from atomic defects in hexagonal boron nitride. Nat Commun 2017;8:705.
[20] Wood JD, Doidge GP, Carrion EA, et al. Annealing free, clean graphene transfer using alternative polymer scaffolds. Nanotechnology 2015;26:055302.
[21] Lin YC, Lu CC, Yeh CH, et al. Graphene annealing: how clean can it be? Nano Lett 2012;12:414–9.

[22] Garcia AG, Neumann M, Amet F, et al. Effective cleaning of hexagonal boron nitride for graphene devices. Nano Lett 2012;12:4449–54.
[23] Wang R, Purdie DG, Fan Y, et al. A peeling approach for integrated manufacturing of large monolayer h-BN crystals. ACS Nano 2019;13:2114–26.
[24] Li X, Zhu Y, Cai W, et al. Transfer of large-area graphene films for high-performance transparent conductive electrodes. Nano Lett 2009;9:4359–63.
[25] Wigger D, Schmidt R, Del Pozo-Zamudio O, et al. Phonon-assisted emission and absorption of individual color centers in hexagonal boron nitride. 2D Mater 2019;6:035006–21.
[26] Feldman MA, Puretzky A, Lindsay L, et al. Phonon-induced multicolor correlations in hBN single-photon emitters. Phys Rev B 2019;99:020101–5.
[27] Scarani V, Bechmann-Pasquinucci H, Cerf NJ, et al. The security of practical quantum key distribution. Rev Mod Phy 2009;81:1301–50.
[28] Sun H, Chen D, Wu Y, et al. High quality graphene films with a clean surface prepared by an UV/ozone assisted transfer process. J Mater Chem C 2017;5:1880–4.
[29] Liu N, Pan Z, Fu L, et al. The origin of wrinkles on transferred graphene. Nano Res 2011;4:996–1004.
[30] Coy Diaz H, Addou R, Batzill M. Interface properties of CVD grown graphene transferred onto MoS2(0001). Nanoscale 2014;6:1071–8.

Supplementary Material: The online version of this article offers supplementary material (https://doi.org/10.1515/nanoph-2019-0099).